Biomechanics and Modeling in Mechanobiology (2018) 17:763–775
https://doi.org/10.1007/s10237-017-0991-6

ORIGINAL PAPER

Effect of rehabilitation exercise durations on the dynamic bone repair process by coupling polymer scaffold degradation and bone formation

Quan Shi[1] · Qiang Chen[1] · Nicola Pugno[2,3,4] · Zhi-Yong Li[1,5]

Received: 3 May 2017 / Accepted: 24 November 2017 / Published online: 8 December 2017

Abstract
Implantation of biodegradable scaffold is considered as a promising method to treat bone disorders, but knowledge of the dynamic bone repair process is extremely limited. In this study, based on the representative volume cell of a periodic scaffold, the influence of rehabilitation exercise duration per day on the bone repair was investigated by a computational framework. The framework coupled scaffold degradation and bone remodeling. The scaffold degradation was described by a function of stochastic hydrolysis independent of mechanical stimulation, and the bone formation was remodeled by a function of the mechanical stimulation, i.e., strain energy density. Then, numerical simulations were performed to study the dynamic bone repair process. The results showed that the scaffold degradation and the bone formation in the process were competitive. An optimal exercise duration per day emerged. All exercise durations promoted the bone maturation with a final Young's modulus of 1.9 ± 0.3 GPa. The present study connects clinical rehabilitation and fundamental research, and is helpful to understand the bone repair process and further design bone scaffold for bone tissue engineering.

Keywords Bone repair · Rehabilitation exercise duration · Scaffold degradation · Bone remodeling · Finite element model (FEM)

1 Introduction

Scaffolds used to repair bone disorders are in increasing need, since the disorders are of great concern due to the increasing aging population. According to the statistics, millions of orthopedic procedures are worldwide performed every year (Lewandrowski et al. 2000). The scaffolds should possess suitable porous structure, mechanical property, biocompatibility, biodegradability, osteoinduction ability, etc. From the biomechanical point of view, mechanical properties of the scaffolds should mimic those of natural bones. In particular, the degradation rate of the scaffolds and the formation rate of bones should match in the repair process, and this is well accepted as a gold standard in the bone tissue engineering (Cao and Kuboyama 2010; Chen et al. 2014; Huang et al. 2014). Otherwise, a stiff scaffold induces the well-known "stress shielding" effect, and a soft scaffold cannot maintain a porous structure in the load-bearing tissue regeneration. Moreover, it was reported that rehabilitation exercise was beneficial to the bone repair (Courteix et al. 1998), but to the best knowledge of authors, the effect of physical exercise durations on the bone repair has not been quantified. Therefore, studying the scaffold degradation/bone formation dynamic coupling process and the influence of rehabilitation exercise durations on the process is necessary.

Biodegradable polymer scaffolds show promise because of their absorbable property, adequate mechanical property and controllable degradation rate (Gopferich 1996), and the polymer degradation can create extra space allowing new

✉ Qiang Chen
chenq999@gmail.com

✉ Zhi-Yong Li
zylicam@gmail.com

1 Biomechanics Laboratory, School of Biological Science and Medical Engineering, Southeast University, Nanjing 210096, People's Republic of China

2 Laboratory of Bio-Inspired and Graphene Nanomechanics, Department of Civil, Environmental and Mechanical Engineering, University of Trento, 38123 Trento, Italy

3 School of Engineering and Materials Science, Queen Mary University of London, Mile End Road, London E14NS, UK

4 Ket Lab, Edoardo Amaldi Foundation, Italian Space Agency, Via del Politecnico snc, 00133 Rome, Italy

5 School of Chemistry, Physics and Mechanical Engineering, Queensland University of Technology(QUT), Brisbane, QLD 4001, Australia

bone in-growth to replace the scaffold eventually. Polymer degradation is due to the scission of long molecular chains caused by hydrolytic reactions and others, and this results in a low molecular weight and mass loss of the polymer. Further, the polymer's structure and physical properties change. At present, there are two erosion mechanisms to describe the polymer degradation. One is surface erosion: as the surface is eroded, the erosion front moves toward the material core (Langer and Peppas 1983); the other is bulk erosion: erosion simultaneously occurs throughout the bulk material. Most numerical analyses of polymer degradation consider the bulk erosion. For example, Gopferich and Langer (1993), Gopferich (1997) theoretically described the bulk erosion by considering a stochastic hydrolysis process. Chen et al. (2011a) proposed a hybrid mathematical model that combined stochastic hydrolysis and diffusion-governed autocatalysis to simulate bulk-erosive biodegradable devices, which showed an excellent agreement with experimental data in literature. However, in reality, the surface and bulk erosions usually coexist or compete (Siepmann and Gopferich 2001; Burkersroda et al. 2002).

Bone tissue growth is under constant and complex remodeling. The remodeling phenomenon can be generally described by the well-known Wolff's law for long bones (Carter et al. 1989; Frost 1964; Huiskes et al. 1987) and for bone repair in tissue engineering (Sturm et al. 2010), and it states that the mechanical stimulation plays an important role in the remodeling process. Based on the concept, researchers developed different bone remodeling theories by applying different mechanical parameters, such as strain, stress or strain energy density. For example, Cowin and Hegedus (1976) firstly proposed a theory of the dynamic cortical bone remodeling, which assumed that the remodeling rate was a linear function of the strain, and trabecula self-adaptably changed till an equilibrium strain state was reached. Carter (1984), Fyhrie and Carter (1986) introduced a 'self-optimization' algorithm based on the strain energy density (SED), which assumed that the mechanical stimulation was proportional to the effective stress field. Later, Huiskes et al. (1987) simplified the algorithm by considering SED rate for bone remodeling. Adachi et al. (2001) used strain gradient and developed a theory assuming that bone formed when the stress of an element was less than the contribution from its neighboring elements; instead, bone was absorbed.

The above introduces the scaffold degradation and the bone remodeling, respectively. Regarding the coupling model, Adachi et al. (2006) and Chen et al. (2011b) combined the hydrolysis-based scaffold degradation theories and bone remodeling theories and developed two scaffold degradation/bone formation coupling models to optimize periodic scaffold architectures, and both showed that different structures had different influences on the coupling process. It is worth mentioning that Chen et al. (2011b) also introduced the auto-catalytic effect, the homogenization technique and topology optimization into the finite element model to find an optimal scaffold structure. However, both degradation models were based on the bulk erosion and did not consider how rehabilitation exercise durations affected the bone repair either.

In the sense of experiments, it is not easy to quantitatively investigate the coupling process. Finite element (FE) analysis as an effective method is often employed to study the relevant issues. It not only provides information about the changes of biomechanical environments after scaffold implantation, but also flexibly incorporates mathematical models for the coupling process, allowing pre-evaluation on how scaffold impacts on the bone repair and further optimal design of the scaffolds.

This study aims to develop a theoretical method to study the influence of the rehabilitation exercise duration per day on the bone repair. First, the scaffold degradation including both bulk and surface erosions is modeled by a stochastic function, which is not influenced by the mechanical stimulation. Different from the degradation, the bone remodeling involving bone resorption and formation is mathematically formulated in terms of SED. Then, by utilizing the FE method and considering different rehabilitation exercise durations per day, the two processes are coupled to study the bone repair process within 200 days after scaffold implantation.

2 Methods

2.1 Numerical implementation

2.1.1 Geometry

A porous periodic scaffold was investigated, as seen in Fig. 1a. Due to the scaffold periodicity, the coupling model of the scaffold degradation and bone formation was formulated based on the scaffold RVC, as seen in Fig. 1b. The RVC was obtained by subtracting three orthotropic and concentric cuboids with identical size $1000\,\mu m \times 600\,\mu m \times 600\,\mu m$ from a cube with side length $1000\,\mu m$. The porosity of the RVC (or scaffold) was calculated as 64.8%, which located in the range of bones' porosity (5–90%, Carter and Spengler 1978).

2.1.2 Materials

After scaffold implantation, the scaffold pores are usually occupied by a fluid. Interstitial fluid (ISF) was observed to mediate signal transduction in mechanical loading-induced remodeling (Hillsley and Frangos 1994); thus, the porous part of the RVC here was assumed to be initially occupied by the ISF. All materials (scaffold, bone and ISF) in the RVC

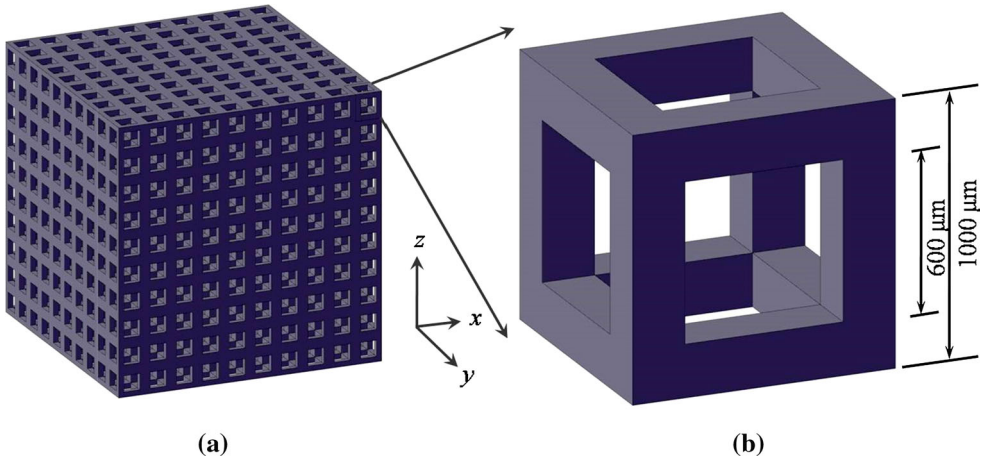

Fig. 1 Periodic scaffold. **a** Scaffold architecture; **b** representative volume cell (RVC)

were assumed to be isotropic and linear elastic, and the ISF was nearly incompressible. The scaffold and bone shared a Poisson's ratio, which was a constant in the entire degradation remodeling process.

2.1.3 Boundary conditions

The RVC bottom surface was fixed, and a rigid plate was placed on the RVC top surface to ensure that the RVC was uniaxially and uniformly deformed in the z-direction. The loading history was a trapezoidal pulse with a period 1 day, and it included relax, ascending, holding, and descending stages, see Fig. 2a. The relax stage t_{relax} meant no exercise, and the rest three stages t_{exercise} described the exercise duration. The cancellous bone is generally subjected to a compressive stress in a range of 0.5–10 MPa (Chen et al. 2011b; Gibson 1985), and as suggested by Shefelbine et al. (2005), the compressive stress on the RVC here was 3 MPa. It is noted that the ascending/descending stages in the loading history were set to be 0.05 day to avoid the abrupt change in the loading history between the relax and holding stages, which might result in an inaccurate simulation. Seven exercise durations, from 0.2 to 0.8 with 0.1 interval, were studied. In the seven durations, degraded scaffold and formed bone were assumed not to fracture.

2.1.4 RVC mesh and simulation

The RVC was meshed into 8000 ($20 \times 20 \times 20$) identical voxel finite elements with side length $l = 50\,\mu\text{m}$, see Fig. 2b. The scaffold degradation and bone formation were numerically performed by coding the user subroutine (VUMAT) of the commercial software Abaqus/Explicit (DS SIMULIA, USA), and the element type was the reduced integration element C3D8R. To display the states of materials assigned to each element during the process, we defined a "state field" χ: namely if $\chi = 1$, the element was scaffold, if $\chi = 2$, the element was bone (including unmatured and matured), and the element was ISF when $\chi = 3$.

2.2 Polymer scaffold degradation

Polylactic acid (PLA) was taken as the constituent material of the scaffold, which is a kind of saturated aliphatic polyesters. In the degradation model, two judgments were used to denote the complete degradation of the scaffold elements. One was based on the polymer molecular weight, which was determined by both bulk and surface erosions; the other was based on a modified stochastic degradation algorithm, which was usually used to describe the hydrolytic degradation of polymers. The two judgments are developed as follows:

2.2.1 Polymer molecular weight

The number average molecular weight M_n of the scaffold element decreases in the degradation process, and $\beta(t)$ is used to describe the degradation degree, which is the ratio of the number average molecular weight $M_n(t)$ of scaffold elements at time t to the weight $M_{n-\text{nd}}$ of the ideal non-degraded scaffold element, i.e.,

$$\beta(t) = \frac{M_n(t)}{M_{n-\text{nd}}} \tag{1}$$

when $M_n(t)$ reduced to a threshold, the scaffold did not have mechanical properties any more. This corresponded to $\beta(t)$ decreasing from 1 to a threshold and indicated that the scaffold changed into the ISF. Moreover, because $M_n(t)$ resulted from the random breakage of polymer chains in the hydrolytic and autocatalytic reactions, the exponential pseudo-first-order kinetics was used to describe the bulk erosion as (Chen et al. 2011a):

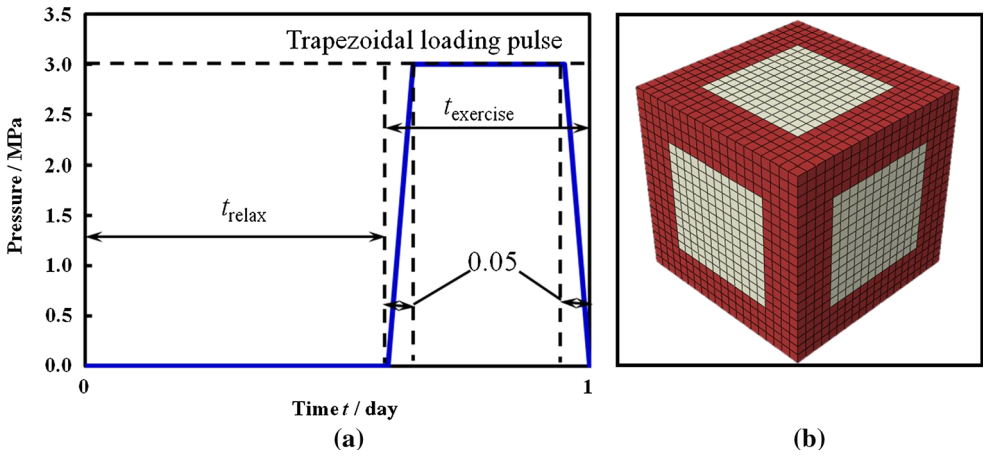

Fig. 2 Exercise duration and mesh of the RVC. **a** Exercise duration described by trapezoidal loading pulse in a day; **b** initial computation domain including 8000 elements, in which the scaffold and ISF elements are red and white, respectively

$$\beta(t) = e^{-\kappa_1 t} \tag{2}$$

where e is the base of the natural logarithm, κ_1 is the bulk degradation rate constant, which is determined by material properties and scaffold morphology, etc. In the ideal case, the polymer at initial stage was non-degraded, and $M_n(0)$=$M_{n-\mathrm{nd}}$ held for all scaffold elements. However, in reality, randomly initial degradation by hydrolysis often occurs in all scaffold elements before implantation; thus, each element had a randomly assigned initial porosity $\alpha = 1-\beta(0)$ (Chen et al. 2011a), which resulted in a initial molecular weight $M_n(0)$=$(1-\alpha)M_{n-\mathrm{nd}}$. Regarding the initial porosity, it was often studied in the drug release kinetics of polymers and varied from 0.2 to 0.7 (Zhang et al. 2003; Ferrero et al. 2003). Here, 0.2 was used as the upper limit, i.e., $0 \le \alpha \le 0.2$. Thus, equation (2) including an additional hysteretic delay t_{add} was rewritten as:

$$\beta(t) = e^{-\kappa_1 (t+t_{\mathrm{add}})} \tag{3}$$

with

$$t_{\mathrm{add}} = -\kappa_1^{-1} \ln(1-\alpha)$$

Equations (2) and (3) only deal with the bulk erosion. However, surface erosion also occurs in the exposed scaffold elements to the ISF. For the surface erosion, the larger contact area between a scaffold element and the ISF, the faster the scaffold element degrades. Therefore, we introduced κ_2 to include the surface erosion, and $f(t)$ represents the number of ISF elements around a scaffold element in a $3 \times 3 \times 3$ zone at time t in the degradation. Based on equation (3), the modified degradation rate was written as:

$$\frac{\mathrm{d}\beta(t)}{\mathrm{d}t} = -\left[1 + \ln\left(1 + \left(\frac{f(t)}{\kappa_2}\right)^2\right)\right] \kappa_1 e^{-\kappa_1 (t+t_{\mathrm{add}})} \tag{4}$$

It is worth mentioning that the local carboxylic acid products play an important role in the autocatalytic effect, and the effect has been verified in the experiments of the local hydrolysis (Wang et al. 2010; Tsuji 2002) and included in a theoretical model (Chen et al. 2011a). However, we here would not take the auto-catalytic effect into consideration. Then, the judgment 1 arrives as:

Judgment 1: The scaffold element ($\chi = 1$) *is completely degraded when* $\beta(t)$ *calculated from equation* (4) *is less than a threshold* β_{thre}, *i.e.*, $\beta(t) < \beta_{\mathrm{thre}}$, *and it is changed into the ISF, i.e.,* χ *from 1 to 3.*

2.2.2 Stochastic degradation

Equation (4) corresponds to a first-order Erlang stochastic process (Gopferich and Langer 1993), and it was used to define the hydrolytic probability density function $p(t)$ of the scaffold element:

$$p(t) = N\left[1 + \ln\left(1 + \left(\frac{f(t)}{\kappa_2}\right)^2\right)\right] \kappa_1 e^{-N\kappa_1 (t+t_{\mathrm{add}})} \tag{5}$$

with

$$N = \ln(n)/\ln(m)$$

where n is the element number per unit volume in the present work, m is the reference element number per unit volume, see Chen et al. (2011a), which influences the degradation rate constant κ_1. According to Gopferich's theory (Gopferich 1997), the complete degradation of a scaffold with a smaller element number in a unit volume needs a longer time than that with a larger element number. Then, the second judgment reads as:

Judgment 2: The scaffold element is completely degraded when a randomly generated number between 0 and 1 is less

than $p(t)$, and it is changed into the ISF, i.e., χ from 1 to 3.

The scaffold element completely degrades when either of the judgments is satisfied. Typically, the mechanical properties of polymers were exponentially related to their molecular weights; for the present model, the Young's modulus $E_s(t)$ of the scaffold element was also exponentially related to $\beta(t)$. Although the experimental result does not show strictly exponential variation, the exponential decrease in Young's modulus is similar to the numerical result by Wang et al. (2010) and experimental result by Tsuji (2002), i.e.,

$$E_s(t) = (E_s - E_{\mathrm{ISF}}) \cdot \frac{e}{e-1}\left(1 - e^{-\beta(t)}\right) + E_{\mathrm{ISF}} \tag{6}$$

where E_s and E_{ISF} are the Young's moduli of the ideal non-degraded scaffold and ISF, respectively. As stated before, for ideal scaffold element without initial degradation (i.e., $t = 0, t_{\mathrm{add}}=0$), we have $\beta(0)=1$, $E_s(0)=E_s$. When the scaffold element is completely degraded at time t, we have $\beta(t) = 0$, and the scaffold element is changed into the ISF, $E_s(t) = E_{\mathrm{ISF}}$.

2.3 Bone remodeling

Bone remodeling under mechanical stimulation is complex, but generally, it consists of bone resorption and formation. It was reported that only the osteoclasts and osteoblasts adhering on the surface of scaffold or bone could sense the mechanical signal (Horwithz and Parsons 1999) and further resorbed and formed bone tissue. Therefore, the bone resorption and formation were considered to only occur on the surface of the scaffold or newly formed bone. In addition, osteoblasts on the surfaces of the extravascular bone matrix (Scheiner et al. 2013) and osteocytes residing in the lacunae (Scheiner et al. 2016a) were directly stimulated by the fluid shear stress, or hydrostatic pressure. However, the structural strain or strain-related stimulation instead of the shear stress or hydrostatic pressure, was widely used to regulate the bone remodeling process. Actually, the strain or strain-related stimulation indirectly influences the cell activities because it causes the changes of the ISF flow and the hydrostatic pressure. Moreover, there is an indication that immature bone is more responsive to alterations of cyclic strains than mature bone (Hou et al. 1990). Thus, the local non-uniform SED ψ was here used as the mechanical stimulus. Based on the Husikes theory (1987) and Schulte's work (2013), the bone remodeling rate $u(\psi)$, indicating the thickness variation of formed/resorbed bone in a unit time, is depicted in Fig. 3, and mathematically expressed as:

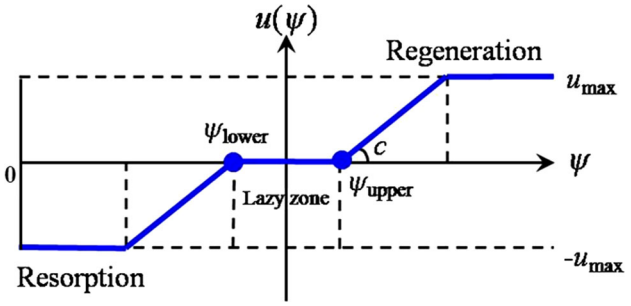

Fig. 3 Bone remodeling velocity $u(\psi)$ versus strain energy density ψ

$$u(\psi) = \begin{cases} -u_{\max} & \psi < \psi_{\mathrm{lower}} - u_{\max}/c \\ -c(\psi_{\mathrm{lower}} - \psi) & \psi_{\mathrm{lower}} - u_{\max}/c < \psi < \psi_{\mathrm{lower}} \\ 0 & \psi_{\mathrm{lower}} < \psi < \psi_{\mathrm{upper}} \\ c(\psi - \psi_{\mathrm{upper}}) & \psi_{\mathrm{upper}} < \psi < \psi_{\mathrm{upper}} + u_{\max}/c \\ u_{\max} & \psi_{\mathrm{upper}} + u_{\max}/c < \psi \end{cases} \tag{7}$$

where c is a constant denoting how fast bone formation and resorption rates reach the maximum growth rate $u_{\max}$, ψ_{upper} and ψ_{lower} are bone formation and resorption thresholds, respectively. Between the two thresholds is the 'lazy zone,' which represents equilibrium between the resorption rate and the formation rate. The local SED ψ of element i is influenced by its neighboring element j within a sensitive distance D, and the closer the jth element to the ith element, the greater it contributes, and the local SED is expressed as (Schulte et al. 2013):

$$\psi(x_i) = \sum_{j=1}^{q} e^{-\frac{\mathrm{d}(x_j - x_i)^2}{2D^2}} \mathrm{SED}(x_j) \tag{8}$$

where q is the number of the contributive elements. $\mathrm{SED}(x_j)$ is the strain energy density of the jth element, and $\mathrm{d}(x_j - x_i)$ is the distance between element i and j. According to the remodeling rate $u(\psi)$, the bone volume fraction $\alpha_b(t)$ of a bone element in the dynamic process increases or decreases, and its rate is defined as:

$$\frac{\mathrm{d}\alpha_b(t)}{\mathrm{d}t} = \frac{u(\psi)}{l} \tag{9}$$

Here, unmatured bone elements are cellular and share a constituent material (matured bone). The bone volume fraction $\alpha_b(t)$ equals $\bar{\rho}_b(t) = \rho_b(t)/\rho_b$, where $\bar{\rho}_b(t)$ is the relative density, which is a primary parameter to determine the Young's modulus $E_b(t)$ of the cellular bone, $\rho_b(t)$ is the density of the unmatured bone, and ρ_b is the density of the matured bone. According to the Gibson's work (1985), the density–modulus relationship $E_b(t) = A\bar{\rho}_b(t)^B$ is employed to describe the Young's modulus of cellular bones (Keller 1994). Meanwhile, considering two extreme cases, $E_b(0) =$

E_{ISF} (i.e., $\bar{\rho}_b(0) = 0$) and $E_b(t) = E_b$ (i.e., $\bar{\rho}_b(t) = 1$), a modified density–modulus relationship is developed as:

$$\begin{aligned} E_b(t) &= (E_b - E_{\mathrm{ISF}})\,\bar{\rho}_b(t)^3 + E_{\mathrm{ISF}} \\ &= (E_b - E_{\mathrm{ISF}})\,\alpha_b(t)^3 + E_{\mathrm{ISF}} \end{aligned} \tag{10}$$

It is worth mentioning that both equations (6) and (10) are empirical, but rigorous solutions can be obtained by employing complex micromechanical models for the mechanical properties of the scaffold degradation (Luczynski et al. 2012) and bone formation (Hellmich et al. 2004; Blanchard et al. 2013).

Like the scaffold degradation judged by molecular weight, the relative density $\bar{\rho}_b(t)$ or bone volume fraction $\alpha_b(t)$ is used to judge the bone remodeling, since it denotes the degree of bone maturation and determines the mechanical properties of bone. Plus, when $\alpha_b(t)$ is small, an element does not contribute to mechanical properties of the scaffold-bone system. Then, this judgment is:

When the bone volume fraction $\alpha_b(t)$ of an element is less than a threshold α_{thre}, the element is changed into ISF (resorption), i.e., χ from 2 to 3. On contrary, when $\alpha_b(t)$ of an element is greater than α_{thre}, the element is changed into bone (formation), i.e., χ from 3 to 2.

3 Results

3.1 Input parameters

The scaffold here was constituted by PLA. The element number per unit volume m in the literature (Chen et al. 2011a) was 100^3, and the counterpart in this work was 2^3, thus, N in equation (5) was calculated as $N = \ln(2^3)/\ln(100^3) = 0.15$. For the bone remodeling, the maximum resorption or formation rate was $2\,\mathrm{mm}^3/\mathrm{mm}^2/\mathrm{yr}$ (Frost 1990), which corresponded to $u_{\max}$=0.005 mm/day in the present simulations. The thresholds ψ_{lower} and ψ_{upper} were modified from literature (Schulte et al. 2013). Besides, as stated in Sect. 2.1, the rehabilitation exercise level was 3 MPa. All input parameters used in the simulation are listed in Table 1.

3.2 Simulation results

In this part, the seven exercise durations and the non-exercise duration were simulated.

3.2.1 The scaffold degradation and bone formation.

The volumes of the degraded scaffold and the formed bone normalized by the RVC volume are plotted in Fig. 4. Generally, it shows the conflict of the trends of the scaffold degradation and bone formation, and the scaffold completely degrades and bone formation reaches a stable state after 140 days. In their respective process, different exercise durations share a trend. For the scaffold, the degradation described by equations (4) and (5) is not influenced by the mechanical stimulation; thus, the degradation for all durations is close to the non-exercise (OSD in Fig. 4a). The degradation difference for all durations after 20 days exists, and this is induced by the coupling of the bone formation, which is remodeled by the mechanical stimulation. For the newly formed bone, bone rarely forms in initial 20 days and reaches a temporary balance before 50 days; afterward, bone keeps forming until

Table 1 Input parameters of the simulations

Parameters		Value	Unit
Bulk degradation rate constant	κ_1	0.0185 (Chen et al. 2011a)	day^{-1}
Surface degradation rate constant	κ_2	6	–
Ratio	N	0.15	–
Constant	c	0.5 (Schulte et al. 2013)	$\mathrm{mmMPa}^{-1}\mathrm{day}^{-1}$
Maximal formation/resorption velocity	$u_{\max}$	0.005 (Frost 1990)	$\mathrm{mm\ day}^{-1}$
Resorption threshold	ψ_{lower}	0.01 (Schulte et al. 2013)	MPa
Formation threshold	ψ_{upper}	0.02 (Schulte et al. 2013)	MPa
Influence distance	D	52 (Schulte et al. 2013)	μm
Young's modulus of mature bone	E_b	20 (Morgan et al. 2015)	GPa
Ideal Young's modulus of undegraded PLA	E_s	5 (Middleton and Tipton 2000)	GPa
Poisson's ratio of scaffold and bone	ν	0.3	–
Young's modulus of ISF	E_{ISF}	0.01	GPa
Poisson's ratio of ISF	ν_{ISF}	0.49	–
State change threshold	α_{thre}	0.01	–
	β_{thre}	0.01	

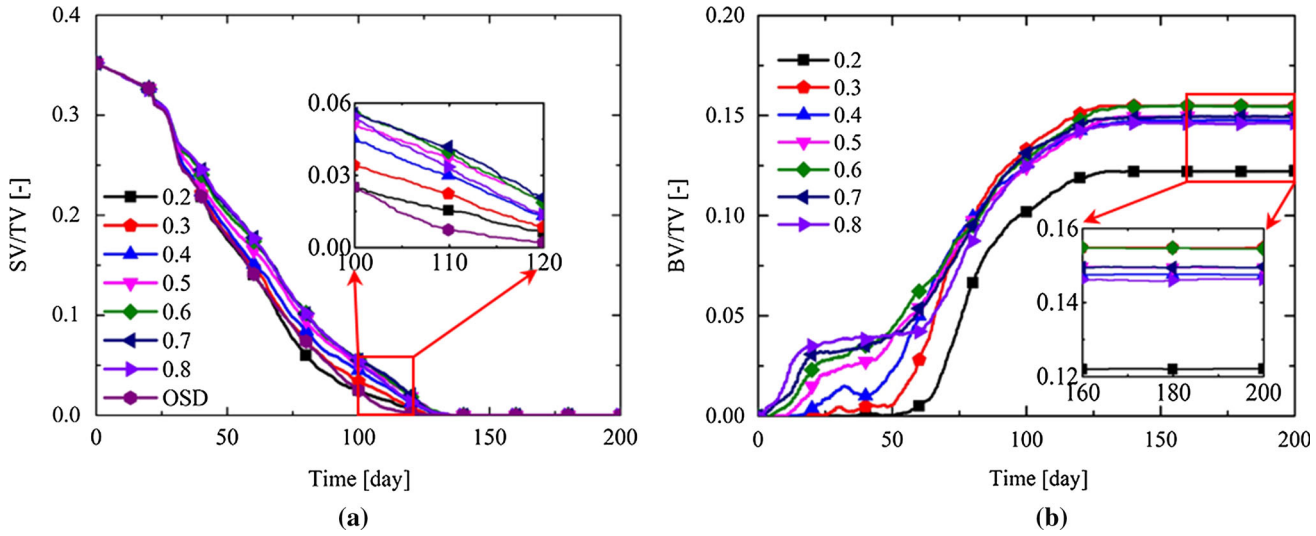

Fig. 4 Changes in SV/TV (**a**) and BV/TV (**b**) with time after scaffold implantation for seven exercise durations and non-exercise duration (only scaffold degradation, OSD). BV: bone volume, SV: scaffold volume, TV: total volume

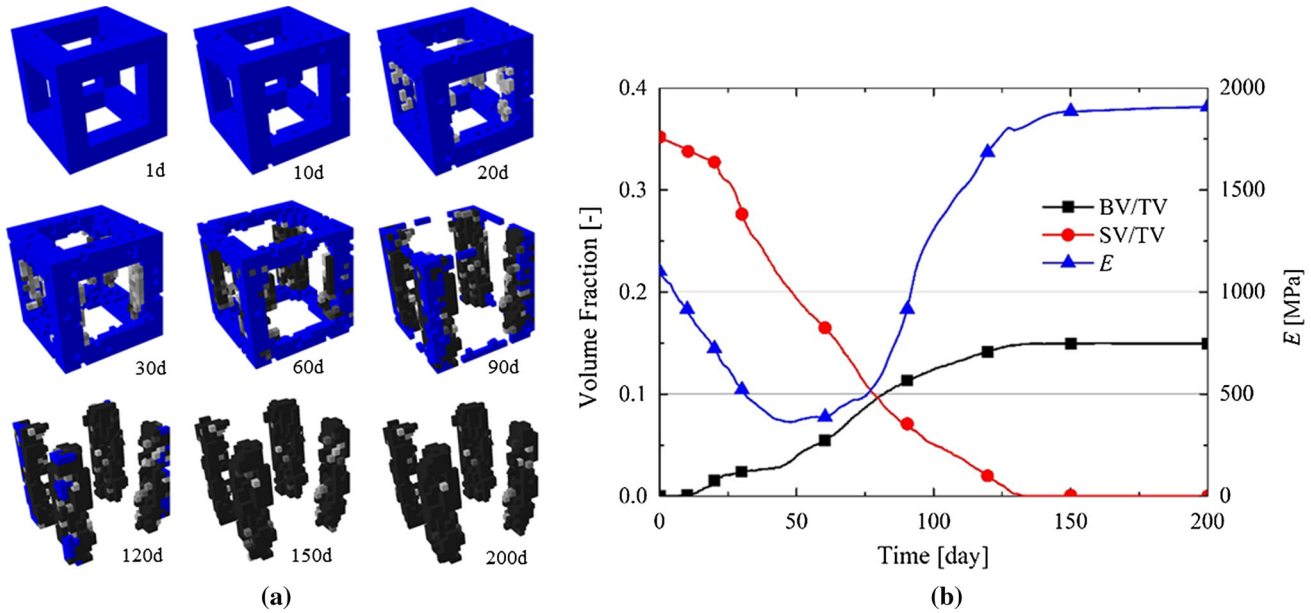

Fig. 5 Coupling process of the scaffold–bone system for the exercise duration of 0.5. **a** Snapshots of the scaffold–bone system at different time points, note that the blue elements are scaffold and others are bone. To observe the maturation degree of formed bone, the bone element is displayed from light gray to dark gray; **b** variations of the Young's modulus, BV/TV and SV/TV

140 days (Fig. 4b). Moreover, the bone forms faster in larger exercise durations than that in smaller durations before the 50th day, while the final bone formation in all durations is similar except for the duration of 0.2.

3.2.2 The coupling process of scaffold degradation and bone formation.

To observe the coupling process, we exemplified the exercise duration of 0.5, and states at nine time points are shown in Fig. 5. For the sake of clarity, Fig. 5 only displays the maturation degree of formed bone by gray values, and the degradation degree of scaffold is shown in Appendix. Before 10 days, scaffold changes weakly (Fig. 5a), and there is almost no newly formed bone tissue (the black dot line in Fig. 5b), but the system's Young's modulus in the loading direction decreases quickly and monotonously (the blue dot line in Fig. 5b). This is because only a portion of PLA molecular chains in the scaffold element breaks (Equation (4)), which results in a decrease in the molecular weight

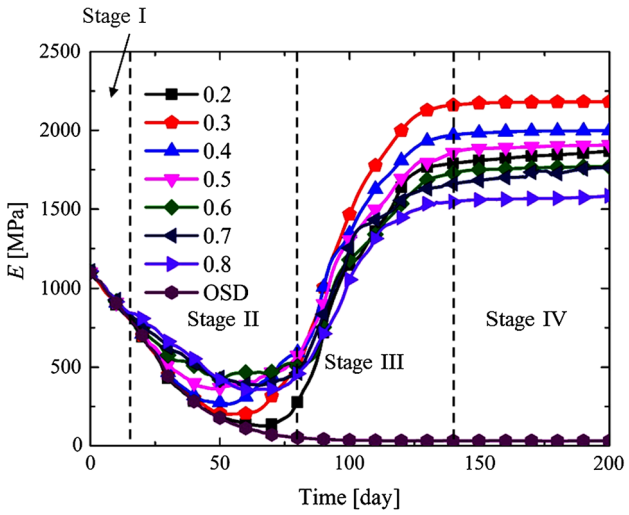

Fig. 6 Young's modulus of the scaffold–bone system under different exercise durations

and a further decrease in Young's modulus of the element. However, this does not mean that the element is completely degraded; thus, the volume of the scaffold element is not reduced significantly (the red dot line in Fig. 5b). From 10 to 60 days, scaffold degrades much faster than before, and more scaffold elements are degraded (Fig. 5a). This is because more and more voids forming in the degraded scaffold facilitate the degradation as the process proceeds. The bone firstly forms on the surface of the four pillars along the loading direction, especially at the eight corners of the RVC because of the high mechanical stimulation. Meanwhile, the Young's modulus of the coupling structure stays constantly around 480 MPa and forms a temporary plateau (Fig. 5b), which roughly corresponds to the temporary balance of the bone formation (Fig. 4b). From 60 to 150 days, the scaffold keeps degrading and almost fully disappears at the 120th day (Fig. 5a), and the fast scaffold degradation promotes the bone formation till the 120th day. Moreover, the Young's modulus increases greatly because of the formed bone. After 150 days, the scaffold completely degrades, and the bone remodeling reaches a balance except few unmatured bone elements.

3.2.3 The comparison of Young's modulus between all durations.

For all the exercise durations, their Young's moduli of the scaffold–bone system are reported in Fig. 6, and they share a variation. According to the specific case in Sect. 3.2.2, we divide the process into four stages. At stage I (0–15 days), there is almost no difference in the Young's moduli between all durations. This is because there is almost no new bone formation, and the scaffold degradation is unrelated to the mechanical stimulation. At stage II (15–80 days), bone starts to form. Different from the degraded scaffold, bone formation is influenced by the stimulation, which results in the disparity between different durations as the process proceeds. At the beginning of this stage, the modulus of the system continues decreasing till the 50th day, after that it rises slightly due to newly formed bone, and the modulus reaches a minimum of the entire process. At stage III (80–140 days), the Young's modulus increases dramatically due to the degraded scaffold, which leads to fast bone formation. At stage IV (after 140 days), the Young's modulus becomes stable due to the completely formed bone. It is worth mentioning that at the stage II, the longer the exercise duration per day, the greater the modulus attains, as shown in Fig. 4b; whereas at the stage III, the system's modulus reverses at the 100th day, i.e., the less exercise duration produces a greater modulus. Regarding the reversal at the stage III, it may be caused by the fast bone formation with greater exercise durations at the stage II, which results in a bone coat around the scaffold, and the coat mitigates the scaffold degradation. Thus, the formed bone under a greater duration is less than that under a smaller duration at the stage III. Interestingly, at the stage IV, the exercise duration of 0.3 has an optimal final modulus, and this indicates that the excessive physical exercise is not beneficial for the bone regeneration.

4 Discussions

The dynamic bone repair process under different exercise durations was investigated and modeled by coupling the scaffold degradation and the bone remodeling. Basic materials were assumed to be isotropic and linear elastic, but the real bone tissue is anisotropic due to the hierarchical arrangement (from nano- to macro-scale) of its components, and the multilevel structure plays a critical role in determining the mechanical properties of the bone (Fritsch and Hellmich 2007; Scheiner et al. 2016b). Materials' anisotropy influences the inter-level or intra-level cracking behavior in the biomaterials–bone system (Scheiner et al. 2016b), and the elastic constants or the strain distribution in an organ after implantation (Hellmich et al. 2008). However, here, due to the only polymer in the scaffold, the polymer was considered as an isotropic linear elastic material. The structural anisotropy of scaffold can be achieved by differentiating the side sizes of the scaffold in its three orthotropic directions, and this could be used to tailor a suitable scaffold to match the anisotropy of macro-level natural bone.

The scaffold degradation is caused by hydrolysis. By adding an extra term $f(t)/\kappa_2$, the surface erosion was incorporated into the model due to surface contact with ISF, which accelerated the degradation. We compared the number aver-

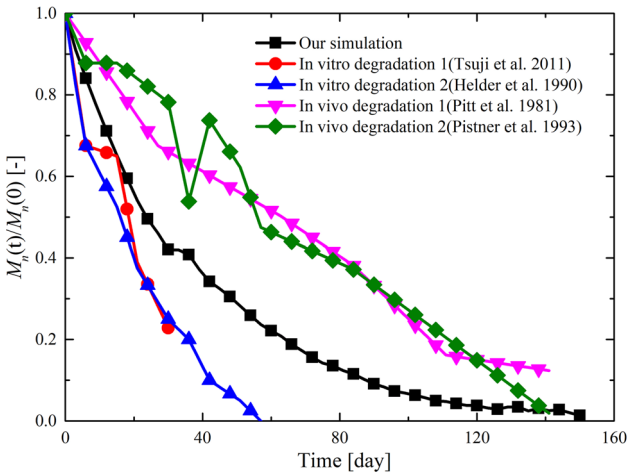

Fig. 7 Comparison between present simulations and measurements: In vitro degradation 1 (Tsuji et al. 2011), in vitro degradation 2 (Helder et al. 1990), in vivo degradation 1 (Pitt et al. 1981) and in vivo degradation 2 (Pistner et al. 1993)

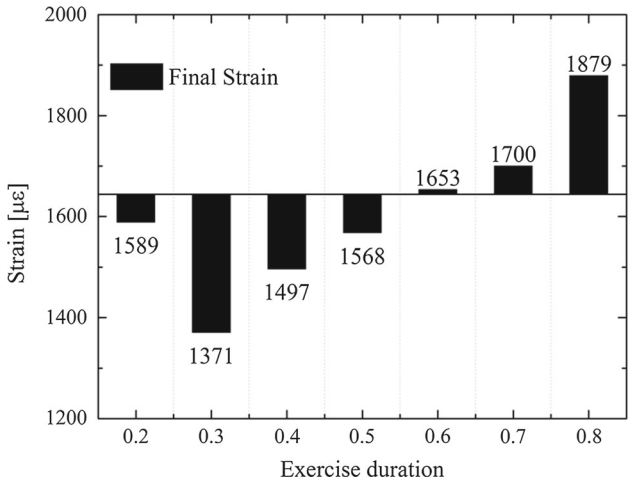

Fig. 8 The final strain of the seven exercise durations

age molecular weight (M_n) in the present simulation with its experimental counterparts from the literature in Fig. 7. Generally, the present degradation exhibits an exponential decay and is comparable to experiments from the literatures (Tsuji et al. 2011; Helder et al. 1990; Pitt et al. 1981; Pistner et al. 1993). In particular, at the early stage of degradation, from 0 to 20 days, the number average molecular weight (M_n) of the scaffold linearly decreased by 40%, while the volume percentage of scaffold in the RVC (SV/TV) only decreased by 10% (Fig. 4a). After 20 days, both M_n and SV/TV decreased until a complete degradation around 150 days. Scaffold's size as well as shape also influences the polymer degradation; thus, they are always optimized from the sense of the physical (mechanics, permeability) and biochemical properties (cell migration, tissue formation). When the size of the PLA matrix is smaller than a critical size, the surface erosion prevails in the degradation process. This is because a larger specific surface area allows a greater contact with water-contained ISF, which facilitates the hydrolytic reaction of the matrix. The scaffold shape seems to have a weak influence on the bone repair dynamic process (McIntosh et al. 2009). However, Adachi et al. (2006) and Chen et al. (2011b) studied two kinds of scaffold RVC with different shapes and reported that the neo-tissue firstly forms at the corner in the former work and on the inner surface in the latter work. This is beneficial for the design of scaffold architectures; for instance, on the basis of the optimized size and shape, the distribution of the polymer mass can be tailored to balance the scaffold degradation and new bone formation (Adachi et al. 2006; Chen et al. 2011b; Hollister et al. 2002). Besides, temperature and pH values of the hydrolytic environment have effects on the degradation rate, and molecular weight also determines the degradation time (Wu and Wang 2001). Thus, the total PLA degradation time differs from 6 months to 2 years (Sinclair 1996), and the degradation parameters in the present simulation could be modified to address different situations.

The bone remodeling is on the basis of a SED-regulated mechanosensory function. At the final stage, the volume percentage of formed bone in the RVC (BV/TV) of all exercise durations, except 0.2, is 15 $\pm$ 1 %, corresponding to an approximate constant porosity of 85% (Fig. 4b). The constant porosity is determined by the geometry (or pillar thickness) of the RVC, and this verifies that the final trabeculae thickness is closely associated with the magnitude of the mechanical stimulation (Ruimerman et al. 2005), and here the applied load was kept to be 3 MPa. The peak strain of the final scaffold–bone system is 1625 $\pm$ 254 $\mu\varepsilon$ (Fig. 8). According to the "mechanostat" model proposed by Frost (2003), the bone remodeling reaches homeostasis, and the remodeled bone mass and strength keep constants when the peak strain is between 1000 $\mu\varepsilon$ and 1500 $\mu\varepsilon$ (Modeling Region, MESm), which is close to the present mean value 1625 $\mu\varepsilon$.

For the coupling model, from Fig. 5a, we can see that there is no formed bone tissue along the horizontal pillars. This is due to the weak mechanical stimulation at the horizontal pillars, which is not able to promote bone formation. This phenomenon is consistent with the numerical simulation by Oers et al. (2008), in which the strain-induced osteocyte signal only directed the bone remodeling in the loading direction. Moreover, this also explains that trabecula in cancellous bone always orientates along the loading direction. From Fig. 6, it is seen that under the same exercise level 3 MPa, the system reaches a minimum state around 50 days and a balance state around 140 days regardless of the exercise durations. This is also comparable to the work by Adachi et al. (2006), who reported that the optimal scaffold was

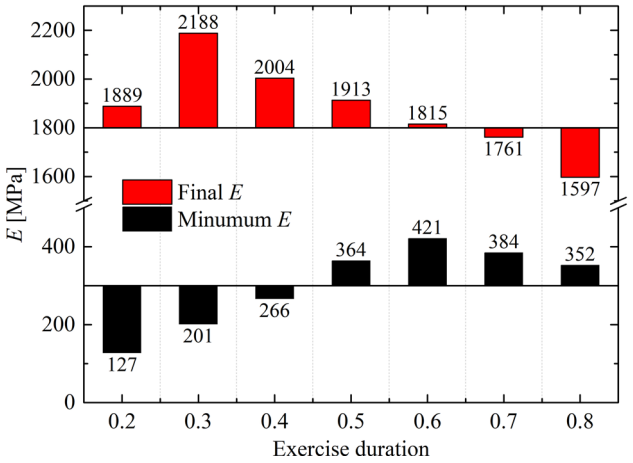

Fig. 9 The smallest and final Young's moduli of the seven exercise durations during the bone repair process

completely degraded after 120 days, and the system's strain energy was the weakest at 40 days. However, it is worth mentioning that they used the strain energy instead of the Young's modulus as the optimal index of the scaffold. In order to monitor the system's Young's modulus in the entire process, the smallest Young's modulus and the final Young's modulus are plotted in Fig. 9, and they are 280 ± 150 MPa and 1900 ± 300 MPa, respectively.

Clinically, the presented results suggest that rehabilitation exercise is unnecessary in the first two weeks as it has slight effect on the bone repair process. After this period, because a longer exercise time produces a smaller final modulus of scaffold–bone system, moderate exercise time is recommended to obtain a final optimal modulus. Here, the exercise duration of 0.3 is the best choice.

Indeed, due to simplifications of the scaffold degradation and bone remodeling, there are limitations. First, in reality, the polymer degradation is also influenced by the mechanical stimulation (Thompson et al. 1996; Fan et al. 2008), composition, molecular weight, shape (Cao et al. 2006) and pH value (Li and Chang 2005), but the present degradation model did not consider these factors. Meanwhile, the polymer degradation here only influences the stress redistribution of the scaffold–bone system, and the effect of the degradation on biological and molecular responses was not taken into account either. Second, the real walking frequency was generally treated as the mean loading history every day due to the computing cost. Thirdly, the mechanical stimulus (SED) was considered as the only factor controlling the bone remodeling. The growth rate c as an empirical constant in equation (7) was selected, whereas actually, the growth rate is related to the biochemical and molecular signals, etc., which regulate the activities of osteoclasts and osteoblasts (Scheiner et al. 2013, 2014). Fourth, ISF was considered as incompressible solid instead of fluid, and this neglects the important role of the fluid shear stress (FSS) between ISF and bone tissue (Dillaman et al. 1991). Despite these limitations, the novel framework still provides insight into the interplay between degraded scaffold and formed bone under different rehabilitation exercise durations and helps establish a sustainable link between the modeling and simulation and the tissue engineering communities.

5 Conclusions

This work investigated the influence of rehabilitation exercise durations on the bone repair process by coupling the scaffold degradation and the bone remodeling, which exhibit an opposite variation. The degraded scaffold dominates the stiffness of the scaffold–bone system at the initial stage, and the newly formed bone dominates at the final stage. Under a cycled mechanical stimulation, excessive rehabilitation exercise duration is not beneficial for the bone repair, and an optimal duration exists. The Young's modulus of the repaired bone tissue is comparable to that of the trabecular bone. Although the theory is based on the simplified mathematical model, it still improves our understanding of the dynamic bone repair process and can be used to guide the rehabilitation exercise and the design of polymer scaffolds for clinical applications.

Acknowledgements This study was supported by the Natural Science Foundation of China (NSFC) (Nos. 31300780, 11272091, 11422222, 31470043, 11772093), the Fundamental Research Funds for the Central Universities (No. 2242016R30014) and partially supported by the National 973 Basic Research Program of China (No. 2013CB733800) and ARC (FT140101152). N.M.P. is supported by the European Commission H2020 under the Graphene Flagship Core 1 No. 696656 (WP14 "Polymer Composites") and FET Proactive "Neurofibre" Grant No. 732344.

Compliance with ethical standards

Conflict of interest The authors declare that they have no conflict of interests.

Appendix

See Fig. 10.

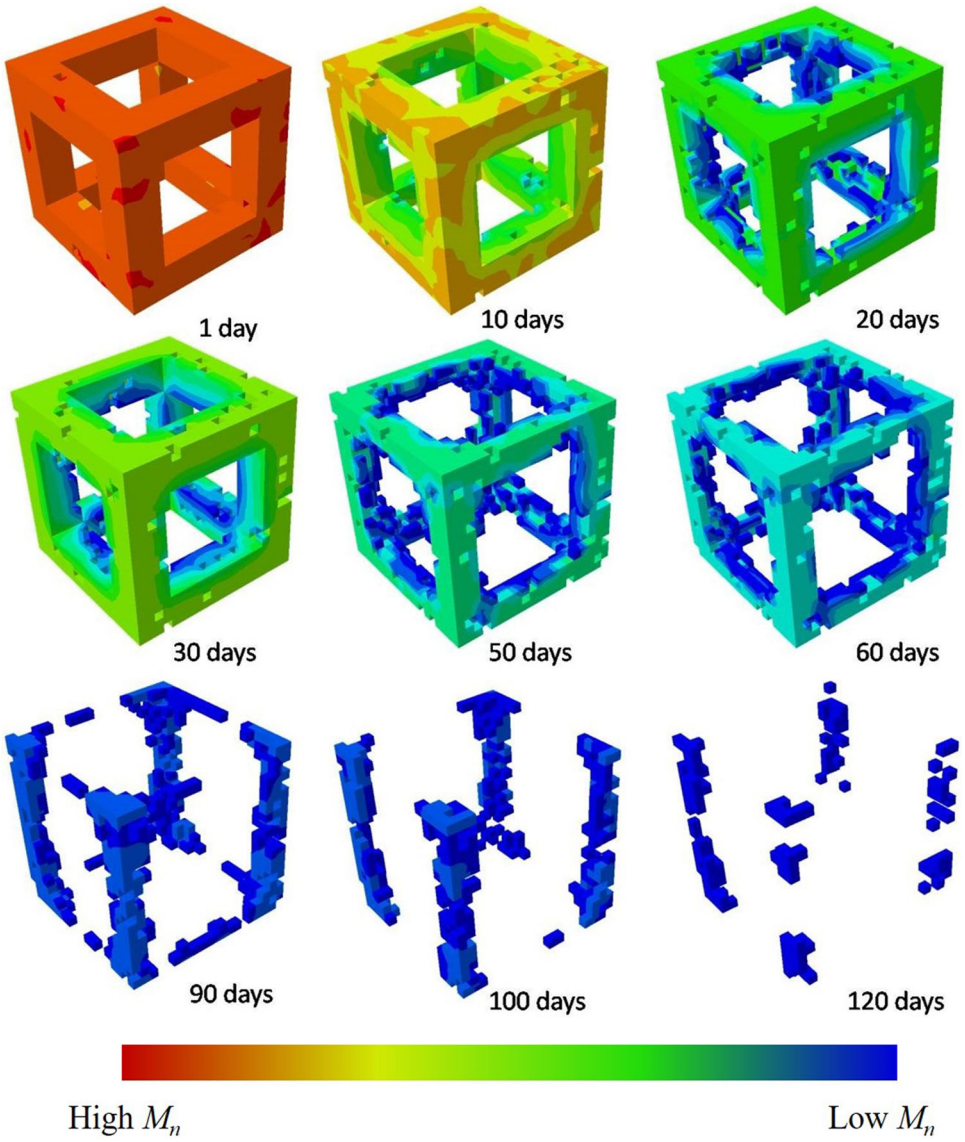

Fig. 10 Snapshots of the evolving process of the degraded scaffold at different time points

References

Adachi T, Tsubota K, Tomita Y (2001) Trabecular surface remodeling simulation for cancellous bone using microstructural voxel finite element models. J Biomech Eng 123(5):403–9

Adachi T, Osako Y, Tanaka M, Hojo M, Hollister SJ (2006) Framework for optimal design of porous scaffold microstructure by computational simulation of bone regeneration. Biomaterials 27(21):3964–72

Blanchard R, Dejaco A, Bongaers E et al (2013) Intravoxel bone micromechanics for microCT-based finite element simulations. J Biomech 46(15):2710–21

Cao H, Kuboyama N (2010) A biodegradable porous composite scaffold of PGA/β-TCP for bone tissue engineering. Bone 46(2):386–95

Cao Y, Mitchell G, Messina A et al (2006) The influence of architecture on degradation and tissue ingrowth into three-dimensional poly (lactic-co-glycolic acid) scaffolds in vitro and in vivo. Biomaterials 27(14):2854–64

Carter DR (1984) Mechanical loading histories and cortical bone remodeling. Calcif Tissue lnt 36:S19–24

Carter DR, Spengler DM (1978) Mechanical properties and composition of cortical bone. Clin Orthop Relat Res 135:192–217

Carter DR, Orr TE, Fyhrie DP (1989) Relationships between loading history and femoral cancellous bone architecture. J Biomech 22:231–44

Chawla AS, Chang TM (1985–1986) In-vivo degradation of poly(lactic acid) of different molecular weights. Biomater Med Devices Artif Organs 13(3–4):153–62

Chen Y, Zhou S, Li Q (2011a) Mathematical modeling of degradation for bulk-erosive polymers: applications in tissue engineering scaffolds and drug delivery systems. Acta Biomater 7(3):1140–9

Chen Y, Zhou S, Li Q (2011b) Microstructure design of biodegradable scaffold and its effect on tissue regeneration. Biomaterials 32:5003–14

Chen Q, Baino F, Spriano S et al (2014) Modelling of the strength-porosity relationship in glass-ceramic foam scaffolds for bone repair. J Eur Ceram Soc 34(11):2663–73

Courteix D, Lespessailles E, Peres SL et al (1998) Effect of physical training on bone mineral density in prepubertal girls: a comparative study between impact-loading and non-impact-loading sports. Osteoporos Int 8(2):152–8

Cowin SC, Hegedus DH (1976) Bone remodeling I: theory of adaptive elasticity. J Elasticity 6:313–26
Dillaman RM, Roer RD, Gay DM (1991) Fluid movement in bone: theoretical and empirical. J Biomech 24(suppl 1):163–77
Fan YB, Li P, Zeng L, Huang XJ (2008) Effects of mechanical load on the degradation of poly(D, L-lactic acid) foam. Polym Degrad Stab 93(3):677–83
Ferrero C, Bravo I, Jiménez-Castellanos MR (2003) Drug release kinetics and fronts movement studies from methyl methacrylate (MMA) copolymer matrix tablets: effect of copolymer type and matrix porosity. J Control Release 92(1):69–82
Fritsch A, Hellmich C (2007) 'Universal' microstructural patterns in cortical and trabecular, extracellular and extravascular bone materials: Micromechanics-based prediction of anisotropic elasticity. J Theor Biol 244(4):597–620
Frost HM (1964) The laws of bone structure. C.C. Thomas, Springfield
Frost HM (1990) Skeletal structural adaptations to mechanical usage (SATMU): 2. Redefining Wolff's law: the remodeling problem. Anat Rec 226(4):414–22
Frost HM (2003) Bone's mechanostat: a 2003 update. Anat Rec 275:1081–101
Fyhrie DP, Carter DR (1986) A unifying principle relating stress to trabecular bone morphology. J Orthop Res 4:304–17
Gibson LJ (1985) The mechanical behaviour of cancellous bone. J Biomech 18(5):317–28
Gopferich A (1996) Mechanisms of polymer degradation and erosion. Biomaterials 17(2):103–14
Gopferich A (1997) Polymer bulk erosion. Macromolecules 30:2598–604
Gopferich A, Langer R (1993) Modeling of polymer erosion. Macromolecules 26:4105–12
Helder J, Dijkstra PJ, Feijen J (1990) In vitro degradation of glycine/DL-lactic acid copolymers. J Biomed Mater Res 24(8):1005–20
Hellmich C, Ulm FJ, Dormieux L (2004) Can the diverse elastic properties of trabecular and cortical bone be attributed to only a few tissue-independent phase properties and their interactions? Biomech Model Mechanobiol 2(4):219–38
Hellmich C, Kober C, Erdmann B (2008) Micromechanics-based conversion of CT data into anisotropic elasticity tensors, applied to FE simulations of a mandible. Ann Biomed Eng 36(1):108
Hillsley MV, Frangos JA (1994) Bone tissue engineering: the role of interstitial fluid flow. Biotechnol Bioeng 43(7):573–81
Hollister SJ, Maddox RD, Taboas JM (2002) Optimal design and fabrication of scaffolds to mimic tissue properties and satisfy biological constraints. Biomaterials 23(20):4095–103
Horwithz AR, Parsons JT (1999) Cell migration-movin' on. Science 286(5542):1102–3
Hou JC, Salem GJ, Zernicke RF et al (1990) Structural and mechanical adaptations of immature trabecular bone to strenuous exercise. J Appl Physiol 69(4):1309–14
Huang S, Chen Z, Pugno N et al (2014) A novel model for porous scaffold to match the mechanical anisotropy and the hierarchical structure of bone. Mater Lett 122:315–9
Huiskes R, Weinans H, Grootenboer HJ, Dalstra M, Fudala B, Slooff TJ (1987) Adaptive bone-remodeling theory applied to prosthetic-design analysis. J Biomech 20:1135–50
Keller TS (1994) Predicting the compressive mechanical behavior of bone. J Biomech 27(9):1159–68
Langer R, Peppas N (1983) Chemical and physical structure of polymers as carriers for controlled release of bioactive agents: a review. J Mater Sci C 23(1):61–126
Lewandrowski KU, Gresser JD, Wise DL et al (2000) Bioresorbable bone graft substitutes of different osteoconductivities: a histologic evaluation of osteointegration of poly (propylene glycol-co-fumaric acid)-based cement implants in rats. Biomaterials 21(8):757–64
Li H, Chang J (2005) pH-compensation effect of bioactive inorganic fillers on the degradation of PLGA. Compos Sci Technol 65(14):2226–32
Luczynski KW, Dejaco A, Lahayne O et al (2012) MicroCT/micromechanics-based finite element models and quasi-static unloading tests deliver consistent values for Young's modulus of rapid-prototyped polymer-ceramic tissue engineering scaffold. Comput Model Eng Sci 87(6):505–28
McIntosh L, Cordell JM, Johnson AJW (2009) Impact of bone geometry on effective properties of bone scaffolds. Acta Biomater 5(2):680–92
Middleton JC, Tipton AJ (2000) Synthetic biodegradable polymers as orthopedic devices. Biomaterials 21(23):2335–46
Morgan TG, Bostrom MP, van der Meulen MC (2015) Tissue-level remodeling simulations of cancellous bone capture effects of in vivo loading in a rabbit model. J Biomech 48(5):875–82
Pistner H, Bendix DR, Muhling J, Reuther JF (1993) Poly(L-lactide): a long-term degradation study in vivo. Part III. Analytical characterization. Biomaterials 14(4):291–8
Pitt CG, Gratzl MM, Kimmel GL, Surles J, Schindler A (1981) Aliphatic polyesters II. The degradation of poly (DL-lactide), poly (epsilon-caprolactone), and their copolymers in vivo. Biomaterials 2(4):215–20
Ruimerman R, Hilbers P, van Rietbergen B et al (2005) A theoretical framework for strain-related trabecular bone maintenance and adaptation. J Biomech 38(4):931–41
Scheiner S, Pivonka P, Hellmich C (2013) Coupling systems biology with multiscale mechanics, for computer simulations of bone remodeling. Comput Method Appl Mech Eng 254:181–96
Scheiner S, Pivonka P, Smith DW et al (2014) Mathematical modeling of postmenopausal osteoporosis and its treatment by the anti-catabolic drug denosumab. Int J Numer Method Biomed Eng 30(1):1–27
Scheiner S, Pivonka P, Hellmich C (2016a) Poromicromechanics reveals that physiological bone strains induce osteocyte-stimulating lacunar pressure. Biomech Model Mechanobiol 15(1):9–28
Scheiner S, Komlev VS, Hellmich C (2016b) Strength increase during ceramic biomaterial-induced bone regeneration: a micromechanical study. Int J Fract 202(2):217–35
Schulte FA, Zwahlen A, Lambers FM, Kuhn G, Ruffoni D, Betts D, Webster DJ, Muller R (2013) Strain-adaptive in silico modeling of bone adaptation-a computer simulation validated by in vivo micro-computed tomography data. Bone 52(1):485–92
Shefelbine SJ, Augat P, Claes L, Simon U (2005) Trabecular bone fracture healing simulation with finite element analysis and fuzzy logic. J Biomech 38(12):2440–50
Siepmann J, Gopferich A (2001) Mathematical modeling of bioerodible, polymeric drug delivery systems. Adv Drug Deliv Rev 48(2–3):229–47
Sinclair RG (1996) The case for polylactic acid as a commodity packaging plastic. J Macromol Sci A A33(5):585–97
Sturm S, Zhou S, Mai YW, Li Q (2010) On stiffness of scaffolds for bone tissue engineering-a numerical study. J Biomech 43(9):1738–44
Thompson DE, Agrawal CM, Athanasiou K (1996) The effects of dynamic compressive loading on biodegradable implants of 50–50% polylactic Acid-polyglycolic Acid. Tissue Eng 2(1):61–74
Tsuji H (2002) Autocatalytic hydrolysis of amorphous-made polylactides: effects of L-lactide content, tacticity, and enantiomeric polymer blending. Polymer 43(6):1789–96
Tsuji H, Eto T, Sakamoto Y (2011) Synthesis and hydrolytic degradation of substituted poly(DL-Lactic Acid)s. Materials 4(8):1384–98
van Oers RFM, Ruimerman R, Tanck E et al (2008) A unified theory for osteonal and hemi-osteonal remodeling. Bone 42(2):250–9
von Burkersroda F, Schedl L, Gopferich A (2002) Why degradable polymers undergo surface erosion or bulk erosion. Biomaterials 23:4221–31

Wang Y, Han X, Pan J et al (2010) An entropy spring model for the Young's modulus change of biodegradable polymers during biodegradation. J Mech Behav Biomed Mater 3(1):14–21

Wu XS, Wang N (2001) Synthesis, characterization, biodegradation, and drug delivery application of biodegradable lactic/glycolic acid polymers. Part II: biodegradation. J Biomater Sci Polym Ed 12(1):21–34

Zhang M, Yang Z, Chow LL et al (2003) Simulation of drug release from biodegradable polymeric microspheres with bulk and surface erosions. J Pharm Sci 92(10):2040–56